Photopumping and fluorescence in a laser-produced plasma. I. Experimental results

C. A. Back and C. Chenais-Popovics
Ecole Polytechnique, Laboratorie de Physique des Milieux Ionisés, 91128 Palaiseau CEDEX, France

R. W. Lee
Lawrence Livermore National Laboratory, P.O. Box 808, Livermore, California 94550
(Received 22 April 1991; revised manuscript received 19 August 1991)

A complete series of three experiments dedicated to the study of a photopumping and resonance fluorescence scheme is presented. An aluminum plasma is preformed in the heliumlike ground state by a 2-J 1.06-μm laser beam, then this plasma is photopumped by an x-ray source $\sim$1 ns later. The pump is a spatially distinct laser-produced plasma that emits intense emission of the heliumlike resonance lines in the 4–8-Å region. The pump is line coincident with the transitions to be photopumped. The resulting perturbation is studied by the fluorescence, which is directly observed and absolutely quantified. The separate characterization of each component of this system is discussed in detail, with an emphasis on the experimental quantities that will be compared with numerical calculations.

PACS number(s): 52.40.Nk, 52.25.Nr, 52.70.La

I. INTRODUCTION

The process of photopumping creates an excited atom or ion by the absorption of a photon. The subsequent relaxation of this induced excited state by spontaneous decay results in fluorescence, the emission of a single photon or several photons, until the atom or ion reaches its original state before the excitation. The nature of the photopumping process is perturbative and it is this character that motivates the present study. In the experiments presented here the photopumping and fluorescence process will be investigated as a probe of a hot dense plasma.

The interest in investigating hot dense plasmas has accelerated greatly since the development of high-powered lasers, as it gave the experimenter more control over the physical conditions of the hot dense matter produced. This control coupled with the advance of diagnostics has led to a steady progress in x-ray spectroscopy. The field of laser-produced plasma studies has evolved from the analysis of pure emission spectra [1–4], which are signatures of the excited-state populations, to the analysis of absorption features [5–8], which provide important insights into the lower levels of the transitions. However, these methods of diagnosing the plasma are largely passive. That is, the plasma emits or absorbs photons and the resulting spectra are recorded.

A diagnostic involving photopumping, on the other hand, is an active method. We use the word "active" because photopumping gives an experimenter the capability to change the plasma state by the introduction of a chosen perturbation. The diagnostic relies on two processes: photopumping and fluorescence. Photopumping is capable of directly perturbing selected states of the ions in a plasma without introducing hydrodynamic perturbations that compete to change the plasma state. Its effect can be monitored by the resulting fluorescence. Hence, photopumping, coupled with fluorescence, can be considered a logical progression of the techniques of plasma spectroscopy.

The present study will attempt to analyze the sensitized fluorescence from a laser-produced plasma. Ideally, a known photon pump can selectively perturb a plasma from one state to another, without modifying the plasma conditions. This would enable the experimenter to monitor the plasma response due to a specified radiative perturbation, its relaxation as well as possible secondary excitations. Thus, the development of such a photon pump will be of particular use in furthering the study of radiative transfer.

To this end, experimental results have been obtained and computer simulations have been performed. The results are presented in two papers that will be referred to as paper I and paper II. In this paper (I) we will present the complete experimental results of a line-coincident photopumping experiment that is optimized to examine the response of a plasma to a perturbing radiation flux. It complements an initial paper that reported the observation of resonance fluorescence (hereafter referred to as BLC) [9]. The following companion paper (II) treats the analysis of the results in more detail by comparisons to an analytic model and a detailed radiative-transfer simulation of the experiment.

The experiments were designed with two main goals in mind. The first objective was to directly observe the fluorescence due to an external photopump. The second was to choose a system, i.e., the combination of photopump and plasma, to create an experimental setup that was as close as possible to a system that could be studied theoretically. This second goal requires that the system be as uncomplicated as possible to emphasize the basic physical processes and to focus on the photopumping itself.

An essential point that we emphasize from the outset is that the tack that is being taken in the present work, and the paper that follows, is outside of the more usual path taken for the study of laser-produced plasmas. In the

more standard approach the diagnostic procedures and the theoretical developments have followed in the footsteps of the desire to achieve some applied goal. The goal may have been inertial confinement fusion, x-ray-laser production, or sources for microlithography, but in all cases, the result was the same—fundamental developments were subordinated to applied goals. In contrast the current work is taking a giant step backwards to return to a fundamental question: Can we understand and predict, in detail, the behavior of a photopumped high-Z plasma?

That this is a step in the opposite direction should be clear from the sheer number of papers on the generation of line-coincident x-ray-laser schemes [10–18]. In the x-ray regime, photopumping originally attracted attention as a possible mechanism to create a population inversion in various x-ray-laser schemes [19,20]. In virtually all the subsequent papers investigating line-coincidence photopumping schemes, the goal is the production of a lasing transition; however, the underlying problems of the developments within the plasma are not of primary interest. Therefore, detailed comparisons between theory and experiment are not undertaken when the scheme proves fruitless; instead a new lasing scheme is proposed. The approach we are taking is rather to begin a systematic study of an experimental design that benefits from both experimental developments and simulations.

To use this type of experiment as a possible benchmark of a radiative-transfer calculation and develop photopumping as a diagnostic, one must try to isolate it from other intervening and indistinguishable physical effects. Therefore, to make the comparison between the simulation and experiment as unambiguous as possible, certain simplifying choices were made.

First, the experimental setup was designed with the goal of producing a one-dimensional system. The important considerations were the target fabrication and the irradiation of the target. The plasma to be pumped was created by irradiating a microdot with a laser focal spot 2.2 times its diameter, so that the resulting plasma is confined by the material in the outer region of the focal spot. This tamping effect serves to collimate the plasma and to reduce the lateral temperature and density gradients [21]. In addition, the pump plasma was created on the opposite side of the target, coincident with the laser axis. Thus the principal axis of change for this one-dimensional system will be along the laser axis, parallel to the normal of the target.

The second significant choice was to experimentally measure the luminosity of the pump instead of relying on a radiative-transfer simulation of the pump to estimate the pumping effect. The pump was resolved as a function of time and spectral composition, and quantified in absolute photon numbers. This eliminates the problem of modeling the radiative transfer of the plasma pumped with input from a radiative-transfer simulation of the pump.

The organization of the paper is as follows. The motivation for the particular experiment of interest is presented in Sec. II. Here the scheme chosen for study in these two papers is described and the particular advantages are highlighted. Although the primary results of the experiments were reported in BLC, a more detailed description will be given here to underscore the importance of the quality of experimental data necessary for comparison with codes, and with the experimental alignment precision required in this type of experiment. Section III presents the first experimental series, which gives the results of absolute measurements of the pump. Section IV describes the second experimental series dedicated to a characterization of the plasma that will be pumped. Section V presents the full two-beam photopumping experiments. Subdivisions treat the procedures taken to ensure that the fluorescence could not be attributed to other sources and presents a range of results obtained. Section VI presents the conclusions.

II. LINE-COINCIDENCE PHOTOPUMPING AND FLUORESCENCE

To maximize the observable fluorescence signal and simplify later simulations, the target of the photopump was chosen to be a K-shell, He-like ion and the pump was chosen to be the photon emission from the He-like lines of the same element. In the experiment described in this paper, the specific pair of photopump transition and transition to be pumped was the Al XII $1\,^1S_0-2\,^1P_1$ transition, which pumped the same heliumlike aluminum transition in a spatially distinct plasma. The populating mechanism is resonant radiative pumping, the process by which the first dipole-allowed excited state is populated by the absorption of photons having an energy equal to the transition energy between a ground and an excited state. The effect of the photopumping will be monitored by the resulting fluorescence.

The advantages of this system as a whole are the following. By choosing the He-like emission from an aluminum plasma as the pump of a spatially distinct aluminum plasma we optimize the energy coincidence between the pump and the transition to be pumped. This obviates the need for a line-coincidence search. There will be, of course, the relative Doppler shifts which we will consider in Sec. V. The resonance line transitions of the plasma to be pumped have extremely strong oscillator strengths and thus the photoabsorption of the pump will be large. In particular, the $1\,^1S_0-2\,^1P_1$ transition is the focus of this study because its oscillator strength is over a factor of 4 larger than those of the other lines, indicating that the photopump will couple most efficiently with this transition. Another advantage in photopumping the $^1P_1$ level is that, again due to the oscillator strength, the radiative decay rate is the dominant deexcitation rate. Since there are no intermediate levels of decay, a maximized fluorescence signal is expected at a single wavelength.

The experimental procedure to unambiguously observe the fluorescence can be considered two stages. The front plasma is first prepared in an initial He-like ground state and then is photopumped by the He-like line emission from a hotter, separate plasma that is created at some later time determined by the experimenter. Thus, the result of photopumping should be an initial null spectrum followed by obvious enhanced emission of photons at the

frequency of the pumped transition when the pump bathes the plasma.

From the experimental point of view, the use of He-like ions offers distinct advantages. First, it is easier to create the He-like ground-state ion in abundance because of the large ionization potential of the ion. Therefore, it is possible to achieve a large population not only of that ion, but also a large population in a particular state, the ground state. This means that the target ion can be dominant over a relatively large temperature regime and, as a bonus, since the ion requires a large amount of energy to reach the first excited state, the self-emission is minimized. The second major advantage arises from the K-shell energy-level structure. The He-like level structure is simpler than that of many-electron ions so that the spectra are amenable to analysis, both qualitatively and quantitatively, since a single line series structure is prominent and the number of overlapping lines is minimized.

In total, three experimental series were performed to demonstrate the photopumping and fluorescence. All were performed at Lawrence Livermore National Laboratory at the JANUS Nd:glass laser facility. During these experiments, JANUS provided two independent laser beams: one having 2 J of 1.064-μm radiation in a Gaussian pulse that was 1 ns full width at half maximum, and the other having 15 J of 0.53-μm radiation in a 100-ps pulse. The rationale behind performing three separate experimental series was to characterize and optimize, within the constraints of the available system, each component of the photopumping system and, having performed this optimization, produce the fluorescence. The first experimental series was performed in order to measure the absolute flux in the pump that would actually be incident on the plasma to be pumped. The second experimental series focused on determining the conditions necessary to create an optimum plasma to be pumped. The third and final experimental series was the full photopumping experimental series.

A diagram of the target used in the complete experiment, in which photopumping will occur, is shown in Fig. 1. Basically, it consisted of a 24-μm-thick substrate of polypropylene, $(C_3H_6)_n$, that had an embedded microdot on one side and a dot on the other. The microdot, a 1500-Å deposit of Al overcoated with 1000 Å of parylene-N, was 270 μm in diameter and served as the target to create the plasma to be pumped. The dot on the other side, 3000-Å thick, was two times the diameter and centered with respect to the microdot. The dot was irradiated later in time to provide an intense photon flux. The flux that traverses the plastic serves as the photopump of the plasma created by irradiating the microdot.

The irradiance conditions are dictated by the guidelines discussed above for creating an experiment which is as one dimensional as possible. The focal spot of 600 μm on the aluminum microdot is 2.2 times greater than the microdot. Irradiating a microdot in this manner creates aluminum plasma that will be confined by the plasma due to the plastic substrate surrounding the microdot. The laser focal spot creating the pump plasma is 270 μm, which is equal to the diameter of the microdot of the front plasma for three reasons: (1) to keep the geometry as one-dimensional as possible, (2) to maintain a high irradiance in the second laser beam, and (3) to ensure that all the photopump photons must traverse in the front plasma, which allows the absolute flux measurements.

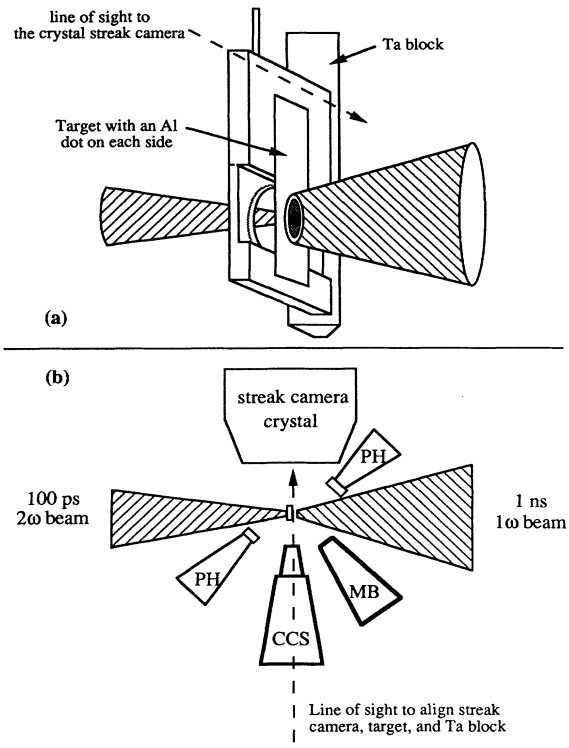

FIG. 1. Setup for the photopumping experiment. (a) Close-up of the alignment of the target showing the line of sight for the streak camera; (b) the diagnostics in the schematic diagram are labeled as follows: pinhole camera (PH), minispectrometer (MB), curved crystal spectrometer (CCS). The Harada grating streak camera (not shown) is 45° out of the plane, above the 1 ns, 1ω beam.

The fabrication of the target itself is a key to these experiments. First, each time the two aluminum plasmas are created the alignment of the laser beams is confirmed by ensuring that the centers of the dots are aligned. Second, the thickness of the target determines the distance between the plasmas; this parameter is measurable to a high accuracy. Thus, the thickness does not contribute to the error involved in the blocking of the pump plasma from the diagnostics. Although the attenuation of the pump by the plastic substrate is undesirable, this geometry allows for two well-defined plasmas which are very close to each other, and yet do not interact with each other hydrodynamically. The proximity of the photon source to the plasma is critical since the flux drops as the inverse of the distance between them squared.

Figure 2 shows a schematic of the target in which the plasma to be pumped and the radiative photon pump are shown. Notice that the front plasma, the plasma that will be pumped, is represented as a column of plasma of the same diameter as the microdot. The absence of la-

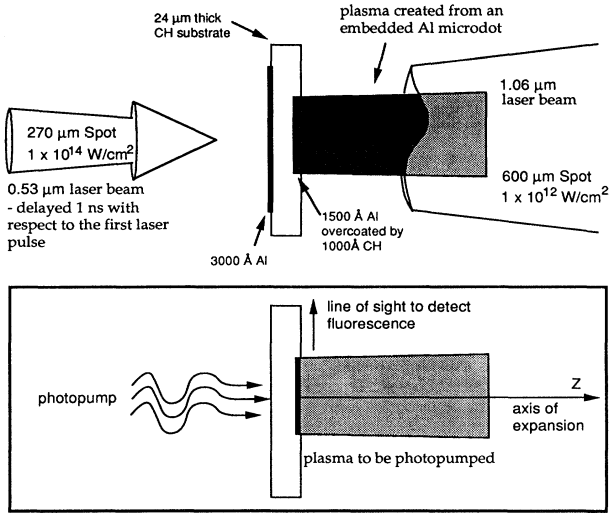

FIG. 2. Schematic design illustrating the laser and target geometry. The front plasma that is photopumped and modeled by a radiative-transfer code is shown. The principal axis of expansion corresponds to the axis that is modeled.

teral expansion is due to the presence of the surrounding carbon plasma created by the laser focal spot which directly irradiates the plastic surrounding the aluminum microdot. The second plasma is represented only as the photons which will photopump the front plasma.

The experimental series will now be discussed in order. The determination of temperatures and densities of the plasmas by spectroscopic analysis using the collisional-radiative code RATION [22] has been presented in the earlier BLC. In this paper, we wish to emphasize those experimental aspects that were not treated fully in the earlier paper, and also to discuss those aspects which bear more directly on the theoretical modeling and simulation.

III. EXPERIMENTAL SERIES I—THE PHOTON PUMP

The purpose of the first experimental series was to characterize the pump plasma and above all measure the absolute number of photons incident on the plasma to be pumped. This experiment was a critical test of the proposed system—if the photon flux proved to be too weak in intensity, then trying to detect fluorescence would be futile. In addition, it was necessary to verify that the pump was well localized. If localized, the pump emission could be obscured so that the spectrometer which would detect the fluorescence would not observe the pump.

The target was a 3000-Å layer of Al deposited on the back of a 24-μm-thick plastic (parylene-E) substrate. It is the same in character as the photopumping target, shown in Fig. 2, except that it does not have the microdot on the other side of the plastic. For the JANUS laser conditions, it was experimentally determined that the Al deposit was thick enough to insure that the plastic substrate behind the aluminum deposit was not ablated during the laser pulse, while the unablated Al was thin enough to minimize the attenuation of the photons that would serve as the pump.

The focal spot used in this experiment was 250 μm in diameter. This diameter was chosen to match the anticipated diameter of the embedded microdot in the final targets. Laser shots at the maximum energy available at JANUS were needed to attain an irradiance of 10^{14} W/cm^2. The laser beam was frequency doubled in order to maximize the conversion efficiency of laser energy into x rays. A 100-ps pulse was used to create a bright burst of x-ray emission that would serve as the radiative pump. The short time duration was chosen to create a well-defined signature in a time that was less than the time scale of the evolving plasma and also to create a radiative source that was localized in space. At 0.53 μm the maximum energy possible was less than 12 J.

The primary diagnostics employed were two minispectrometers to record the absolute photon flux from the back and front of the target simultaneously. They will be referred to as MA and MB, respectively. Both used pentaerythritol (PET) crystals to diffract the x rays in the range of 5 to 8 Å. The spectra were recorded on Kodak Direct Exposure Film (DEF). Detector MA viewed the side on which the laser was incident. The detector MB was placed on the opposite side. It measured the x rays that were transmitted through the plastic substrate of the target—the flux that the microdot would actually receive if it were in place. In addition, pinhole cameras recorded the size of the x-ray-emitting region of the plasma.

As noted in BLC, a consistent determination of the temperature and density taking into account all the measurements indicates that the plasma produced had a temperature in the range of 400 to 600 eV and an electron density in the range of 5×10^{19} to 5×10^{21} cm^{-3}.

Additional analysis of experimental series I was performed to determine the shape of the pump line emission. Since the spectrographs did not have a high enough resolution, an estimate of the profile is deduced by considering linewidths in the same spectral region and the line intensity ratio of Al XIII $1\,^2S_{1/2}-2\,^2P_{1/2}$ to Al XII $1\,^1S_0-2\,^1P_1$ in the following manner.

First, the source size was determined from the width of the intercombination line, the $1\,^1S_0-2\,^3P_1$ transition, on the film. This line is spectrally pure, so the contributions of overlapping, unresolved lines do not cause artificial broadening. By knowing the geometry of the spectrometer and the rocking curve, the size of the emitting source can be calculated. The measurement indicated a source size of 250 to 300 μm.

Second, the widths of the higher-order lines were broadened relative to the intercombination line, therefore an indication of the density could be determined by Stark broadening. Since the spectra were considered unresolvable at principal quantum number $n=6$, the Al XII $1\,^1S_0-5\,^1P_1$ transition was used to deduce the density.

The following equation is a fit to the Stark width of the Al XII $1\,^1S_0-5\,^1P_1$ transition, which is determined by calculations using the quasistatic and electron-impact approximations [23]:

$$\Delta\omega\ (\text{eV})=0.14+[1.25+1.67T\ (\text{keV})]\times\left[\frac{n_e}{10^{21}}\right]^{0.59-0.17[T\ (\text{keV})-0.3]}$$

This equation is parametrized as a function of electron temperature T_e and electron density n_e for the relevant range observed in the experiment. It is accurate to within 5% for temperatures 100 to 700 eV and densities 5×10^{20} to 5×10^{22} cm^{-3}. The instrumental width $\sim$2 eV convolved with the profile does not significantly affect the fit. The measured values for the width of this line are on the order of 8 eV, indicating an electron density of $\sim10^{22}$ cm^{-3}, which is consistent with the n_e determined by the line ratios.

Time-resolved data shows that the maximum emission of the $n=2$ resonance line occurs at the same time as the $n=5$ resonance line emission. Space-resolved data taken later in experimental series III that the maximum emission originates from the same spatial region. Hence, the line broadening calculations provide an estimate of the Stark width of the $n=2$ to 1 transition at the same temperatures and densities as determined for the $n=5$ to 1 transition. The width due to Stark broadening scales approximately as n^4, where n is the principal quantum number of the upper state. Therefore, calculations indicate that the upper limit on the Stark width of the $1\,^1S_0-2\,^1P_1$ resonance line is always less than the Doppler width for the transitions, which are 0.3 to 0.8 eV for these temperatures. Therefore, for the pump plasma, the line shape is best represented by a Doppler profile.

The resolution of the time-integrated spectrometer was not high enough to resolve the broadening due to optical depth effects; however, by examining the line ratios we can conclude that they do affect the spectra. Since gradients affect the individual line intensities differently, diagnostic line ratios involving the optically thick He-like resonance line should bracket the plasma parameter regime present in the experiment. In the temperature and density regimes consistent with previous estimates, the He-like intensity ratios involving the satellites were considered the most reliable line intensity ratio diagnostics since these lines are optically thin and are localized in the volume of plasma that provides the bulk of the pump emission. When the temperature and density determined from line ratios using the optically thin satellites transitions are compared with those temperatures and densities derived from ratios using the He-like resonance line it is found that the latter diagnostic deviates in a manner consistent with a ratio involving an optically thick emission line. This behavior then implies that the emission line profile was broadened.

These factors, i.e., the Stark width, source size, temperature, and optical depth, taken together lead to the conclusion that the He-like resonance line $1\,^1S_0-2\,^1P_1$ will be well represented by a opacity broadened line profile with Doppler wings.

The absolute flux calculation will be treated in more detail as it will be used as an initial condition in any theoretical model. The absolute flux is the most difficult measurement experimentally, yet the most important. In order to extract meaningful numbers for the absolute flux, the crystals were calibrated and x-ray film was developed according to prescribed procedures. The crystals were calibrated using a stationary anode source at Lawrence Berkeley Laboratory [24]. The cold aluminum $K\alpha$ line emission (1486 eV) dispersed by the crystal was recorded by a proportional counter and compared with the directly measured signal. The integration of the signal scanned over angle gives a measure of the crystal rocking curve. The measures were 0.3 ± 0.4 mrad. They deviate from the values for an idealized crystal by 35%. Great care was taken with the film since the published absolute calibration of the film in photons/μm^2 is valid only under the condition that its development is strictly monitored. During the experiments, the development of the film took place in a temperature controlled darkroom using chemicals that were changed daily. The film was developed according to the standards given by Henke [25].

Figure 3 shows a plot of the absolute flux in the He-like resonance line as a function of laser energy. Note that the flux that traverses the plastic substrate of the target is actually measured. This flux will be the true photopumping flux that irradiates the front plasma. For laser energies in the range of 5 to 12 J the absolute number of photons derived from the time-integrating spectrometer, which directly measured the pump plasma only, were on the order of 1.0×10^{13} to 3.0×10^{13} W/cm^2. The photons/sr actually incident on the front plasma were measured to be $\approx2.0\times10^{12}$. The decrease in the absolute flux at higher laser energies is probably due to a degradation of the beam quality at high energies.

Measurements of the x-ray transmission through the CH substrate were within 3% of the transmission predicted by the attenuation calculated from mass absorption coefficients of cold CH. This result indicates that the CH substrate *between* the two microdots remains intact during the two laser pulses and the material properties of the CH do not appreciably change. Therefore, for this geometry and target, the conversion efficiency of incident laser light to the photon pump will be similar to backlight sources which are traditionally measured from the same side as the incident laser. In the event that one cannot perform detailed pump measurements it is therefore important to note that the present results indicate that the measured front flux can be scaled to give the flux that passes through the plastic and serves as the pump.

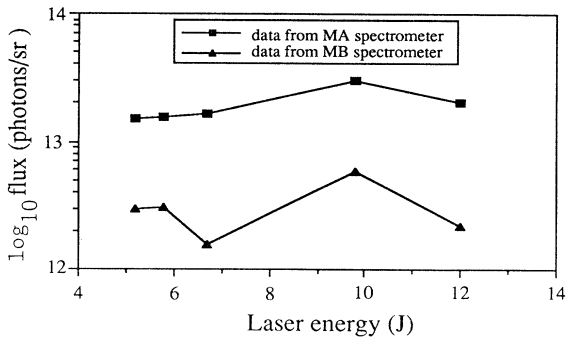

FIG. 3. Photons per steradian of the pump plasma in the $^1S_0-^1P_1$ emission line of aluminum. The flux from the same side (MA) as the incident laser is compared with the flux on the opposite side that traverses the plastic substrate of the target (MB).

IV. EXPERIMENTAL SERIES II—THE PLASMA TO BE PHOTOPUMPED

The second experimental series was performed specifically to determine optimal laser conditions for the creation of the He-like plasma that will be photopumped. Essentially, this translates to determining the laser energy needed for minimum emission of He-like Al lines because threshold emission indicates the population of the He-like aluminum ground state is large. Since the ideal case of no self-emission is difficult to achieve, the time dependence of the emission was determined to select the optimal time to photopump. When the optimal conditions were found, the temperature and density of the plasma were measured by the use of the line intensity ratios of lines in the 20–60-Å regime.

The target was a microdot, 270 μm in diameter, deposited on a 24-μm foil of plastic (polypropylene) and overcoated with 1000 Å of parylene-*E*. The irradiance conditions for the front plasma were a 1-ns laser beam at 1.06-μm wavelength in a 600-μm-diam focal spot. Fairly low energies of about 2 J were sufficient to create the He-like Al plasma, with a minimum of He-like emission.

The diagnostics used to monitor the front plasma were a crystal streak camera and a flat-field Harada grating streak camera. For this experiment, both streak cameras were mounted perpendicular to the laser axis. The crystal streak camera used a potassium hydrogen phthalate (KAP) crystal and covered a wavelength region of 5 to 8 Å with a resolving power of $\sim$200. This crystal streak camera monitored the emission from the hydrogenlike and heliumlike ion stages of aluminum. The Harada grating streak camera covered a range of 20 to 60 Å. This latter spectrograph primarily recorded the emission from the lithiumlike aluminum ions as well as the hydrogenlike and heliumlike emission of carbon. The carbon emission originates from the plastic which is directly ablated by the laser. This plastic is used to tamp the hydrodynamic expansion of the aluminum plasma located in the interior of the irradiated focal spot. The Li-like emission was monitored because it shows that the plasma was sufficiently ionized to create a significant population of He-like ground-state aluminum ions.

To determine the proper condition, the following method was used. First the microdot was irradiated and the He-like plasma was seen in emission. The focal spot, as discussed in the introduction, was fixed to be larger than the microdot. Therefore, the laser energy was decreased until the emission could not be detected or was barely detectable by the principal spectrograph, the crystal streak camera.

During this series of shots we recorded the emissivity of the heliumlike resonance line, which is an indication of the desired initial state, to the total energy on target. A distinct increase was found in emission of the resonance line for laser energies between 2 and 3 J. The variation of the peak resonance line emission showed a factor of 7 to 25 increase in this energy range. Based on these results, the optimal laser conditions were determined to be a laser pulse at 1.06 μm with less than $\sim$2.5 J of energy.

Figure 4 shows the time-resolved data of the He-like emission in the 4–8-Å range and the emission in the 30–50-Å range which is predominantly Li-like; these data were taken with the streak spectrometers. The strong Li-like emission indicated that the plasma was hot enough to create a sizeable He-like ground-state population when the He-like emission on the crystal streak camera is minimized.

The temperature and density of the plasma were determined by line ratios from the Li-like and He-like lines arising from the $n=2$ states. While these ratios are functions of both temperature and density—thus are not ideal diagnostics—these ratios are sufficient to bracket the plasma conditions. Moreover, since a microdot was used, the margin of error is smaller than those for a plasma created from a solid target in which the gradients span a larger range. Line intensities from the Al XII and Al XI stages were used to determine the following front plasma line ratios: $I(3\,^1P_1-2\,^1S_0)/I(4\,^2D_{1/2}-2\,^2P_{1/2})$, $I(3\,^1P_1-2\,^1S_0)/I(3\,^2D_{1/2}-2\,^2P_{1/2})$, and $I(4\,^2D_{1/2}-2\,^2P_{1/2})/I(3\,^2D_{1/2}-2\,^2P_{1/2})$. The temperature inferred from these ratios is in a range of 200 to 400 eV, and the electron density is in the range from 5×10^{20} to 1×10^{21} cm^{-3}.

The ideal initial plasma condition with no He-like emission was difficult to achieve because of inhomogeneities in the beam and fluctuations in the laser energy. A plasma that is too hot has strong self-emission that makes the fluorescence difficult to detect. On the other hand, a plasma that is not hot enough does not have a sufficient number of He-like ions in the ground state. Given the difficulty of creating a He-like plasma with no self-emission, the time necessary for the extinction of the He-like resonance signal was measured with the streak camera. At the end of the detectable self-emission, there will exist an abundance of He-like ions in the ground state since the time required for recombination to occur into the Li-like ion is typically on the order of nanoseconds for the plasmas studied here. Thus, the optimal time to introduce the photopump is after the end of the self-emission. Analysis of the data indicated that a time delay of 1 ns from the creation of the plasma was sufficient to separate the self-emission from the expected fluorescence signal.

V. EXPERIMENTAL SERIES III–THE PHOTOPUMPING EXPERIMENT

The full photopumping experiment is a synthesis of the first two experimental series. The objective is to directly observe fluorescence due to photopumping. The results presented in BLC will be reviewed briefly and further we will discuss more fully the two main results as they are the basis for the comparison to simulations. The two main results are the ratio of the self-emission to the fluorescence signal and the absolute flux of the fluorescence signal. The ratio was determined by time integrating the time-resolved streak camera data. The absolute flux, quantified in absolute number of photons per steradian, required both the time-resolved and time-integrated data. We will also present a brief discussion of possible processes, other than photopumping, that could cause the

second signal observed, which is interpreted as fluorescence.

During the two-beam experiment, the beams irradiated opposite sides of a planar target. A 1-ns beam of 1.06-μm wavelength at 1.0×10^{12} W/cm^2 was used to prepare the front plasma in the Al XII ion stage. A 0.53-μm wavelength laser beam with a 100-ps pulse length created the pump plasma. An irradiance of 1.0×10^{14} W/cm^2 was used to generate x rays in the pump plasma. Both laser beams were focused and aligned with $f/4$ lenses by viewing the target in retroreflection. The temporal peak of the laser beam that created the radiative pump was delayed by $\sim$1.0 ns relative to the peak of the first laser pulse. A 600-μm focal spot was used to create the front plasma and a 270-μm focal spot was used to create the pump plasma.

Figure 1 shows the experimental setup. All the instruments previously described in experimental series I and II were fielded in this experiment. One of the time-integrating crystal spectrometers MA was replaced by a curved crystal spectrometer with a space-resolving slit of 25 μm; this is indicated as CCS in the figure. Two pinhole cameras were also used to monitor the consistency of the laser focal spots.

Now since two laser plasmas are created, the relative motional Doppler shift must be considered. The Doppler shifts of the pump plasma and the plasma to be pumped can be estimated by considering the experimental conditions and target fabrication. The time duration of the laser beam that created the pump was deliberately chosen to be short, 100 ps. Space-resolved measurements of the plasma show that the peak of the He-like resonance line emission of the pump takes place at the surface of the target. The bulk of the photopumping emission comes from the dense region that is essentially stationary during the period of fluorescence and no appreciable Doppler shift is expected.

The pumped plasma, on the other hand, does experience a motion relative to the stationary target. At the time of the pump, a velocity gradient will exist in the plasma along the axis of the laser. Since the absorption

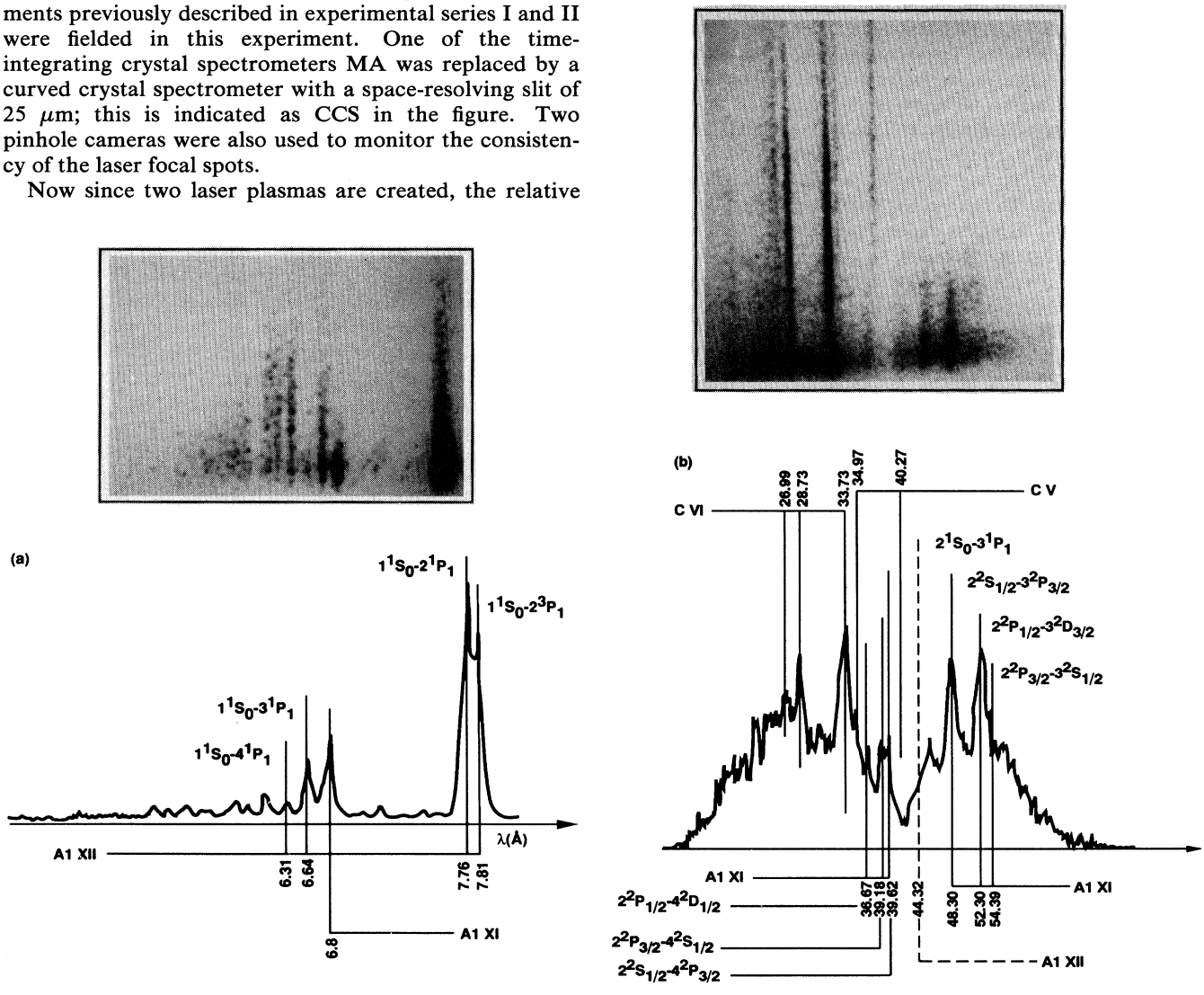

FIG. 4. Time-spectrally-resolved data recorded on x-ray streak cameras. (a) 4–8-Å wavelength region, (b) 20–60-Å wavelength region. The minimized emission of the He-like ions coupled with the strong emission of the Li-like ions indicates that the population of He-like ground-state ions is dominant.

depends exponentially on the density, the region that will have the highest absorption is the region having densities greater than the critical density and a temperature of <100 eV. This region will have a velocity less than the speed of the critical surface. Certainly, velocities greater than that of the critical surface are present in the underdense plasma, and the resulting velocity difference may render the pump ineffective. However due to the target fabrication, the first layer of the target to be ablated by the laser is the plastic overcoat. Hence, it can be reasonable assumed that there is no aluminum plasma having velocities greater than 3×10^7 cm/s. Since the region experiencing the highest absorption is the most important, we estimate a velocity shift approximately equal to the velocity of the critical surface. Thus for a plasma having a temperature of 150 eV, the velocity difference is $\sim3\times10^6$ cm/s, which corresponds to a wavelength shift of 9×10^{-4} Å. This is factor of ~2 less than the Doppler half-width of the pump line.

A. Competing sources of emission during the fluorescence

There are two sources of emission that could potentially compete with the fluorescence signal: (1) the self-emission coming from the plasma itself as a result of the excitation by the laser, and (2) the pump source if viewed directly. The tactics to ameliorate these problems are described below.

The self-emission occurs during the initial formation of the plasma. It can be separated from the fluorescence by introducing a delay between the two laser pulses which causes a shift in time between the peaks of the fluorescence and the self-emission. The time resolution is crucial to separate the two periods of emission. Thus, the primary diagnostic was time resolved, an x-ray streak camera that uses a KAP crystal as a dispersing element. The sweep speed used was 65 ps per millimeter to allow the two signals to be temporally resolved and yet appear within the total time frame of the diagnostic, which is limited by the active photocathode dimensions.

In the second case, the pump emission occurs at the same time as the expected fluorescence. Since the pump and the fluorescence emission are of the same wavelengths, the pump emission must be eliminated from view otherwise the pump emission and fluorescence could not be differentiated. In this experiment the pump and plasma to be pumped are spatially distinct. This fact permits the use of a physical obstruction to block the solid angle of the pump from the primary diagnostic. To eliminate the pump emission, a shield of tantalum was used to block it from the diagnostic.

To insure consistency, the results of the first two experiments were confirmed. This procedure allowed us to check the laser conditions and characterizations of each of the two plasmas. Next, two-beam shots were performed to create both plasmas without the Ta block, in order to adjust the timing and verify the line overlap of the He-like $^1S_0-{}^1P_1$ transition of the back and front plasmas. Figure 5 is a reference spectrum from the principal diagnostic, the crystal streak camera, which shows the overlap of the initial spectrum and the pump spectrum. The Ta shield is not used in this shot. The relative magnitudes from this shot are not relevant because the laser energies were changed to record both sets of emission with the same streak camera gain. What is important is that it shows the position of the relevant spectral lines on the streak camera which does not change when the shield is in place. The figure shows that the range of spectral lines observed encompasses the He-like series as well as the H-like lines of aluminum.

Preliminary shots were taken to test both the alignment procedures and the effectiveness of the tantalum block. In particular, one-beam shots to create the radiative pump blocked by the Ta shield were performed. These shots were critical to proving that the Ta block shielded the crystal streak camera from the pump emission and thus proved that the fluorescence observed was not a direct emission from the radiative source. The streak camera data showed no He-like Al or H-like Al emission, while data from spectrometers that were not blocked verified that the emission was present. These shots did indicate that stray light amplified by the streak camera or continuum emission can be a problem. Using these data the sources and relative amplitude of background emission could be bracketed.

B. Identification of the fluorescence signal

After the confirmation of the above, the photopumping experiments were performed. In contrast to the reference spectrum shown above, it is important to realize that when the shield is added, the streak camera only registers the emission from the pumped plasma. In BLC, Fig. 2, the reduction of the raw data to give the $1\,{}^1S_0-2\,{}^1P_1$ intensity as a function of time is shown. The first peak is the self-emission created by the first laser pulse. The second peak occurs during the photopumping. As noted, at these low emission levels the total signal includes background which is subtracted to yield the true signal. A

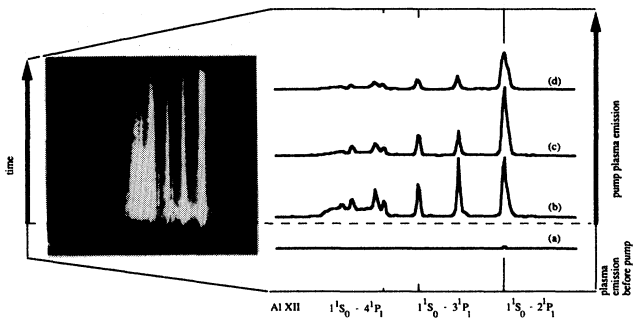

FIG. 5. Reference spectrum on the crystal streak camera in which the front and the pump plasma emission are both visible. The time axis is in bold after the creation of the pump. The front plasma is created by a 1.9-J, 1-ns pulse, focused into 600 μm, the pump is created by a 3.2-J, 100-ps pulse focused into 270 μm. (a) Self-emission of the plasma before the pump; (b) self-emission and pump emission at the peak of the pump; (c) 0.27 ns after the peak; (d) 0.53 ns after the peak.

complete range of fluorescence signals are shown in Fig. 6.

The second peak behaves as the fluorescence signal should. First, while tests of the pump plasma with the shield were deliberately done to insure the pump was blocked from the streak camera, in actuality it can be verified in each shot that the pump is not directly observed. In Fig. 6, the enhancement of the He-like resonance line emission is seen, but not of the other lines, in particular, the H-like lines. This absence is proof that the pump is not directly seen, because otherwise all the emission lines of the pump should be seen. Second, the growth of the signal is not due to scattering alone since that should cause an enhancement of all the lines in the spectrum without preference for the He-like resonance line. Third, a further confirmation that the signal is

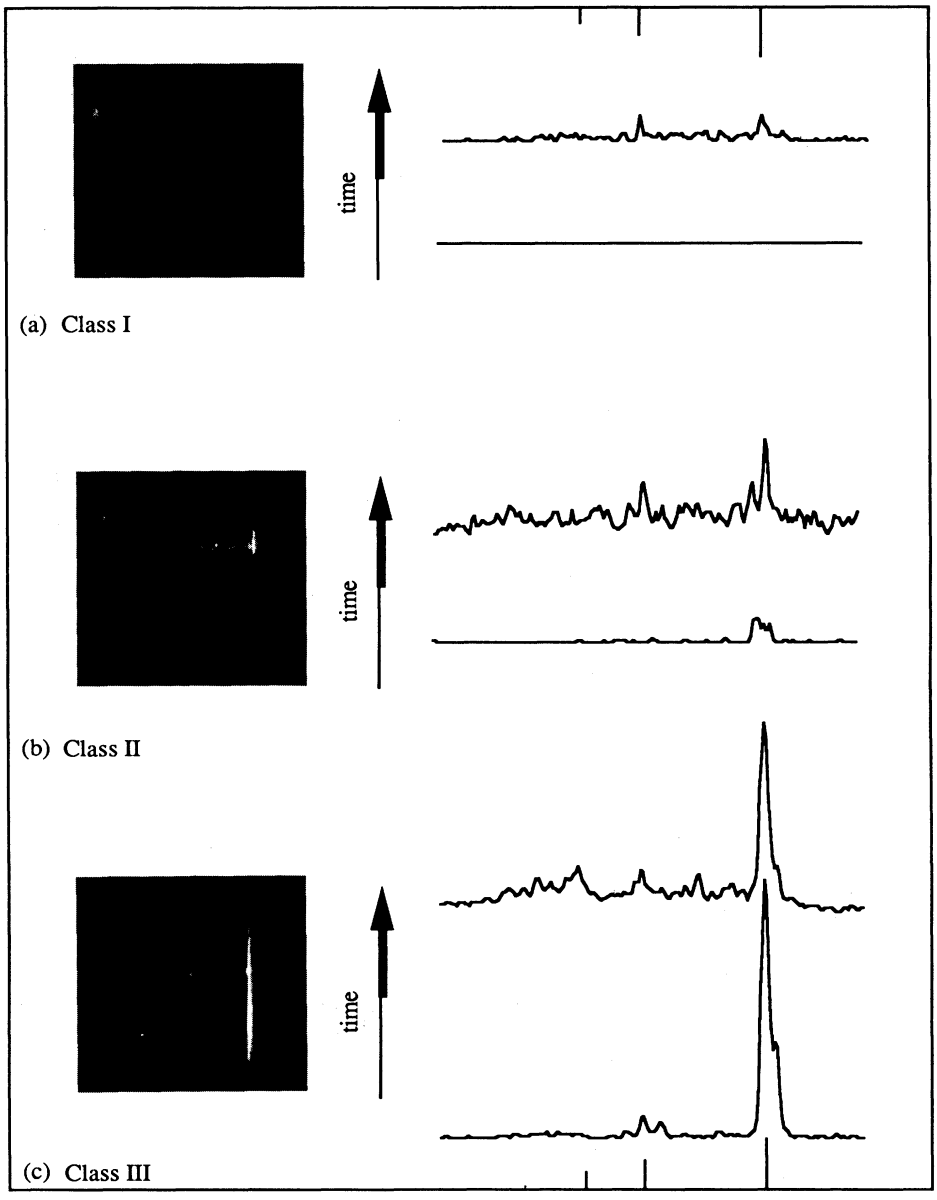

FIG. 6. Photographs of the raw data and the corresponding spectra showing the sensitivity of the fluorescence signal to the front plasma conditions. The time axis is shown in bold when the pump turns on. (a) Class I: little or no self-emission, the fluorescence is weak; (b) class II: self-emission that dies out before pump, the fluorescence signal is well separated in time; (c) class III: strong self-emission, the fluorescence appears on the tail.

indeed the fluorescence is that the increased intensity of the resonance line emission coincides with the onset of the photon pump.

Figure 7 shows lineouts of the intensity of the He-like resonance line as a function of time for the different experiments in which photopumping was observed. All data have been corrected for the background as described above. The intensity scales are arbitrary. The weaker shots, i.e., Figs. 7(c) and 7(d), display a distinct fluorescence signal but these are noisy due to the subtraction of the background.

Other mechanisms that could cause the second peak involve processes that bulk heat the plasma. For instance, a shock produced by the pump laser beam might cause significant heating. Such a shock would travel at about the speed of sound through the CH substrate, 10^6 cm/s. Therefore, for the target used in these experiments, the shock transit time would be ~ 2.5 ns. The fluorescence signal appears after ~ 1 ns, too early to attribute the signal to the heating of the front plasma by a shock front.

Another possibility is that the time-delayed laser beam heats the front plasma since the laser beam that creates the pump plasma irradiates the back side of the target. This possibility is obviated for these targets since care was taken to ensure that the laser did not ablate the entire deposit of aluminum in the bare microdot. Moreover, the CH substrate was 24-μm thick. Hence, the possibility of direct heating of the front plasma by the laser beam that created the pump plasma was eliminated by the target design. Thus, other possible interpretations of the second emission peak are considered improbable.

C. Classification of results according to the initial plasma state

A striking feature of the fluorescence results is the sensitivity of the photopumping to the state of the front plasma. Based on the behavior of the time-resolved He-like resonance line intensity, these shots can be divided into three classes shown in Fig. 6: (1) No appreciable self-emission and little or no photopumping (a), (2) weak self-emission from the front plasma which dies off before the pump radiation (b), and (3) strong self-emission which does not die off before the fluorescence (c).

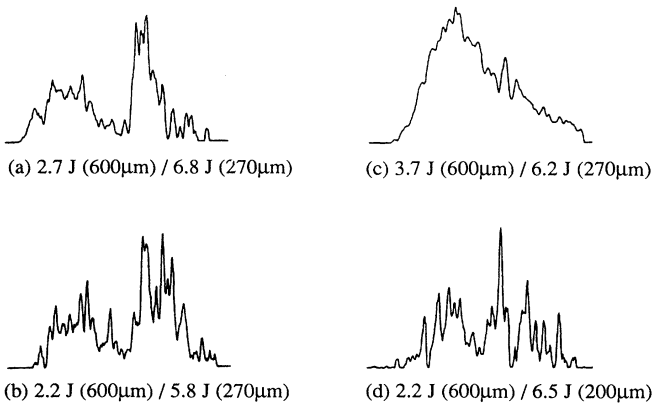

FIG. 7. Intensity traces of the Al XII resonance line as a function of time. The first peak is due to the self-emission; the second peak is due to the fluorescence emission. (a) class II, (b) class II, (c) class III, (d) fluorescence resulting from a pump plasma that is smaller in diameter than the microdot.

In the first class, the front plasma was not ionized enough to have a sufficient population of excited He-like ions to generate a detectable signal. Therefore, the self-emission is absent. Further, there is a small population of heliumlike ground-state ions so that the photopumping was ineffective. These conclusions are confirmed by the weak of emission from the Li-like ions which was recorded simultaneously on the Harada grating streak camera.

In the second class, only the Al XII resonance line is distinctly observed in self-emission and fluorescence. The Al XIII lines and other Al XII lines are not detected even though they lie in the measured spectral range. The lack of strong emission in the other He-like lines indicates that the excited-state population of He-like ions is small and the emission is not detectable.

The lineout in Fig. 7(a) is the clearest example of the fluorescence signal because it is well resolved in time from the self-emission. The self-emission peaks at roughly the same time as the laser pulse, then dies out before the pump plasma is created.

The probability for analyzing the fluorescence signal is greatest for plasmas in this class. Indeed, the data shows a fluorescence signal that is well resolved in time from the self-emission. The lineout in Fig. 7(b), which comes from a plasma that had laser parameters similar to those for the lineout in Fig. 7(a), shows a similar character. The fluorescence signal is weaker, but is still significantly higher than the noise.

In the third class, the He-like Al resonance line is still observed in emission when the photopumping begins making the fluorescence signal more difficult to distinguish. In the lineout in Fig. 7(c) the energy in the front plasma was 30% higher creating a higher temperature plasma. In this case, the self-emission does not end before the fluorescence signal appears. The maximum intensity of the resonance line emission for this shot is a factor of 10 higher, relative to the others shown; the fluorescence appears as a bump on the tail of the self-emission.

The Al XII $3\,^1P_1-1\,^1S_0$ line is present also. This line transition in the front plasma is not expected to couple to the radiative pump as strongly as the resonance line because its oscillator strength is lower by a factor of 4 compared to that of the $2\,^1P_1-1\,^1S_0$ transition. A lineout of the Al XII $3\,^1P_1-1\,^1S_0$ line does show some slight evidence of photopumping, but the signal is very noisy, and difficult to quantify.

The last lineout, Fig. 7(d), is of an experiment with virtually the same laser energies as class II, but the focal spot of the pump laser 200 μm, smaller by a factor of 26% in diameter. In this shot, the photopumping is not as effective because the radiative pump did not entirely cover the microdot.

To summarize we find that the second peak in this data can be unambiguously attributed to the fluorescence effect. The two-beam shots of experimental series III re-

vealed that the photopumping is very sensitive to the front plasma conditions. The optimal plasma to photopump was created by a laser beam having a laser energy of 2 J. The fluorescence was observed to have a full width at half maximum of 200 ps, which is about twice the photopumping laser full width at half maximum, and the fluorescence starts at the onset of the photopump.

In general, the signals were not strong. The weakness of the initial ambient emission is expected because of the plasma state. However, the intensity of the fluorescence signal could be diminished by the blocking effect of the Ta shield. Because the alignment of the block was crucial to eliminating the spectra from the pump, the shield was placed conservatively so that it may have blocked part of the fluorescing volume of the front plasma. Blocking the pump plasma was absolutely critical to the experiment, therefore the tendency in alignment was to overcompensate by obscuring part of the front plasma emission.

D. Ratio of the self-emission to the fluorescence ξ

To reduce the experimental data for comparison directly with the simulations, the crystal streak camera data was used to determine a ratio ξ defined as the time-integrated signal due to the self-emission divided by the time-integrated signal due to the fluorescence. The ratio is a measure of the relative strength of the fluorescence to the self-emission and since it is recorded on a single instrument, cross calibration is not necessary. If the ratio is less than 1, then the predominant emission of the resonance line that was pumped occurs during the fluorescence. Conversely, if the ratio is greater than 1, then the self-emission dominates the fluorescence. The smallest ratios determined in these experiments is on the order of ~ 1.

In Table I the focal spots and energies of the two-beam photopumping shots are given. The first three cases correspond to the raw data shown in Figs. 6. In cases where the self-emission did not end before the fluorescence, an extrapolation of the self-emission tail was used.

To insure that the integration of the signal was not skewed by an erratic sweep speed the uniformity of the streak camera sweep was tested. In addition, tests were performed on the actual CsI photocathode used during the experiments. These indicated that the cathode had a uniform coating, indicating that imperfections in the cathode did not affect the results.

TABLE I. The laser energy (J), pump focal spot diameter (the front focal spot diameter was 600 μm), and ratio ξ for the photopumping shots.

Laser energy $\lambda=1.06$ μm	Pump focal spot μm	Laser energy $\lambda=0.53$ (μm)	Ratio
1.0	600	5.4	a
2.7	270	6.8	1.00
3.7	270	6.2	3.34
2.2	200	6.5	1.12
2.2	270	5.8	0.92

[a]There was no self-emission on this shot.

E. Absolute flux of the fluorescence

During the photopumping experiment, the flux incident on the plasma could not be directly measured. Therefore, based on the results of experimental series I, the direct flux of the pump plasma was measured and then used to infer the flux incident on the front plasma by correcting for the attenuation of radiation due to the CH substrate between the pump plasma and the plasma pumped.

During the photopumping shots, the MB minispectrometer was used to record the absolute flux of photons detected in the fluorescence signal. The analysis of the absolute photon number due to the fluorescence signal is based on the absolute photon number from the radiative pump and the ratio of the integrated fluorescence signal to the self-emission signal from the streak camera.

First, we consider the radiation that reaches the minispectrometer. The aspect ratio of the target is such that the diameter of the spots are a factor of 100 larger than the distance between them (see the Fig. 2 for the geometry), so the pump radiation reaching the minispectrometer, which is positioned at an angle of 54° from the laser axis, must pass through the front microdot plasma. The lateral spreading of the emission region is assumed to be minimal and this is verified by pinhole images of the source size.

The total emission recorded on the minispectrometer is the sum of three quantities: the emission from the back-plasma pump I_{pump} which is attenuated by the CH and Al from the front microdot T_{CH} and T_{Al}, respectively, the self-emission from the front plasma I_{front}, and the fluorescence signal I_{fluor}. Thus,

$$I_{\text{total}}=I_{\text{pump}}T_{\text{CH}}T_{\text{Al}}+I_{\text{front}}+I_{\text{fluor}} .$$

Note that I_{pump} has already been corrected to represent the radiation that is incident on the microdot, that is, the measured pump flux has already been attenuated by the CH of the substrate.

This equation can be simplified as follows: For the front plasma, the absorption coefficient of the resonance transition can be estimated using the optical depth of the transition at the line center of a Doppler profile,

$$\tau=n_e\frac{\pi e^2}{mc}f_{ij}\Phi(0)l ,$$

where n_e is the electron density, f_{ij} is the absorption oscillation strength, $\Phi(0)$ is the profile at line center, and l is the length of the plasma. For a plasma having a temperature of 200 eV and an electron density of 1.0×10^{21} cm^{-3}, $\tau/l\approx2\times10^5$ cm^{-1}. Therefore, the pump photons are absorbed within the first 0.2 μm of the front plasma. Then the transmission of the pump flux through the Al microdot is reduced to zero and the term involving I_{pump} in the total detected flux goes to zero.

An upper limit on the total fluorescence emission is determined by assuring that all the radiation absorbed

from the back pump is emitted to 4π. The amount absorbed then reemitted would be

$$I_{\text{fluor}} = \frac{I_{\text{pump}}}{4\pi} .$$

The measurement from the experimental data gives $I_{\text{pump}} \sim 2.0 \times 10^{12}$ photons/sr.

In addition, the collisional deexcitation rate is on the order of 10^{11} cm^3/s for the resonance transition. So the probability of photon destruction, i.e., that the photons are absorbed into the thermal energy pool, expressed as the ratio of the collisional deexcitation to the total collisional and radiative deexcitation is on the order of 0.0001. This indicates that a photon absorbed near the center of the embedded microdot will probably be lost to the thermal pool and not detected by the streak camera.

To complete the equation for the I_{total} we use a relationship between the integrated fluxes of the self-emission and the fluorescence derived from the streak camera data. The streak camera gives the ratio of integrated flux of the self-emission to the integrated flux of the fluorescence.

The equation, rewritten in terms of the ratio ξ defined in Sec. V D gives

$$I_{\text{total}} = I_{\text{front}} + I_{\text{fluor}} = I_{\text{front}} \left[1 + \frac{1}{\xi} \right] .$$

Here, we assume that the emission is essentially isotropic so that the difference in the angle of observation by the streak camera and minispectrometer is not critical.

This equation is used to determine the number of photons in the fluorescence signal. Thus, the absolute flux of the fluorescence signal was found to be $\sim 1.5 \times 10^{11}$ photons/sr, which represents an upper limit of the absolute flux of the fluorescence.

VI. SUMMARY AND CONCLUSIONS

The photopumping of the $^1S_0 - ^1P_1$ transition in heliumlike aluminum has been demonstrated by detection of fluorescence. A line-coincidence scheme was used because of its twofold advantage: (1) the large ionization potential provides a wide range of temperature over which the $^1S_0$ heliumlike ground-state ions can exist without significant emission of the He-like and H-like lines, and (2) the heliumlike resonance line has a large absorption coefficient. Together, these factors assist in producing a scheme in which it is possible to isolate the fluorescence.

The experimental section presents a description of three experimental series dedicated to the study of this problem. Because a true study of photopumping depends on studying the results of the perturbation of an initial state, it is essential to characterize the individual plasmas, both the initial state and the pump. Therefore, the separate experimental series which determine the plasma parameters of the pump and plasma to be pumped are absolutely necessary to interpret the photopumping data. The planar target configuration, having an aluminum deposit on each side, allows the plasmas, which are extremely close spatially, to be fully studied by diagnostics.

The primary importance of the first experimental series was to show that a plasma could serve as an x-ray pump and perturb a different plasma. The previous development of backlight sources for use in studying laser-produced plasmas was a significant help to this part of the work. The second experimental series determined the optimal combination of laser irradiance conditions and target configuration necessary to produce an ionized plasma that could be photopumped. A delicate balance between creating a system that was ionized to the proper state and yet had a minimum of self-emission in the fluorescing line was achieved. Here, embedded microdots helped to minimize the temperature and density gradients in the plasma.

The final fluorescence experimental series involved a combination of the procedures described above. The front plasma, the one to be pumped, was created first and the radiative pump plasma was created 1 ns later. Time-integrated and time-resolved diagnostics recorded the spectra. The key diagnostic enabling the observation of the fluorescence was an x-ray crystal streak camera to time resolve the emission used in conjunction with a Ta block to shield this streak camera from the direct pump flux.

The pump plasma was created by irradiating the target with a 0.53-μm wavelength laser beam having 5 to 12 J of energy in 100 ps. The analysis showed that the pump plasma had a temperature in the range of 400 to 600 eV and electron densities in the range of 5×10^{19} to 5×10^{21} cm^{-3}. The front plasma was created with a laser beam having ≤ 4 J of energy at 1.06 μm in 1 ns. The temperature was found to be 200 to 400 eV and the electron density was in the range of 5×10^{20} to 1×10^{21} cm^{-3}.

The emission of the transition that was photopumped increased during the photopump. In general, a first peak occurs at the peak of the laser pulse that initially created the plasma while a second peak occurs during the photopump flux. Conclusive tests were performed to show that the second peak could not be attributed to the direct observation of the radiative pump. Other sources of heating were considered, and were found to be insufficient to cause the second emission peak. On the time-resolved data the fluorescence signal distinctly appears and is sensitive to the initial state of the plasma.

The absolute photon flux of the fluorescence was deduced to be on the order of 1.5×10^{11} photons/sr. This calculation depends on the measurement of the absolute photon flux delivered by the radiative pump and on the ratio of the self-emission to the fluorescence measured by the streak camera. This quantitative measurement of the fluorescence is an upper limit on the fluorescence.

ACKNOWLEDGMENTS

We would like to thank in particular the people who provided technical support for this series of experiments: Jim Swain, W. Cowens, R. Wallace, S. Mrowka, G. Glendinning, J. Kilkenny, and B. Stewart. This work was performed under the auspices of the U.S. Department of Energy by Lawrence Livermore Laboratory under Contract No. W-7405-Eng-48.

[1] V. A. Boiko, A. Ya. Faenov, and S. A. Pikuz, J. Quant. Spectrosc. Radiat. Transfer **19**, 11 (1978).
[2] J. H. Key, C. L. S. Lewis, J. G. Lunney, A. Moore, J. M. Ward, and R. K. Thareja, Phys. Rev. Lett. **44**, 1671 (1980).
[3] P. G. Burkhalter, M. J. Herbst, D. Duston, J. Gardner, M. Emery, R. R.Whitlock, J. Grun, J. P. Apruzese, and J. Davis, Phys. Fluids **26**, 3650 (1983).
[4] A. Zigler, H. Zamora, N. Spector, M. Klapisch, J. L. Schwob, and A. Bar-Shalom, J. Opt. Soc. Am. **70**, 129 (1980).
[5] J. Balmer, C. L. S. Lewis, R. E. Corbett, E. Robertson, S. Saadat, D. O'Neil, J. D. Kilkenny, C. A. Back, and R. W. Lee, Phys. Rev. A **40**, 330 (1989).
[6] C. Chenais-Popovics, C. Fievet, J. P. Geindre, J. C. Gauthier, J. F. Wyart, and E. Luc-Koenig, Phys. Rev. A **40**, 3194 (1989).
[7] A. Hauer, R. D. Cowan, B. Yaakobi, O. Barnouin, and R. Epstein, Phys. Rev. A **34**, 411 (1986).
[8] D. K. Bradley, J. Kilkenny, S. J. Rose, and J. D. Hares, Phys. Rev. Lett. **59**, 2995 (1987).
[9] C. A. Back, R. W. Lee, and C. Chenais-Popovics, Phys. Rev. Lett. **63**, 1471 (1989) (referred to as BLC).
[10] P. Hagelstein, Plasma Phys. **25**, 1345 (1983).
[11] J. Krishnan and J. Trebes, Appl. Phys. Lett. **45**, 189 (1984).
[12] J. P. Apruzese and J. Davis, Phys. Rev. A **31**, 2976 (1985).
[13] R. C. Elton, T. N. Lee, and W. A. Molander, Phys. Rev. A **33**, 2817 (1986).
[14] D. G. Goodwin and E. E. Fill, J. Appl. Phys. **64**, 1005 (1986).
[15] B. N. Chichkov and E. E. Fill, Opt. Commun. **74**, 202 (1989).
[16] Y. T. Lee, W. M. Howard, and J. K. Nash, J. Quant. Spectrosc. Radiat. Transfer **43**, 335 (1990).
[17] T. Boehly *et al.*, Phys. Rev. A **42**, 6962 (1990).
[18] J. Nilsen, Phys. Rev. Lett. **66**, 305 (1991).
[19] A. V. Vinogradov, I. I. Sobel'man, and E. A. Yukov, Kvant. Elektron. (Moscow) **2**, 105 (1975) [Sov. J. Quantum Electron. **5**, 59 (1975)].
[20] B. A. Norton and N. J. Peacock, J. Phys. B **8**, 989 (1975).
[21] M. J. Herbst, P. G. Burkhalter, J. Grun, R. R. Whitlock, and M. Fink, Rev. Sci. Instrum. **53**, 1418 (1982); M. J. Herbst and J. Grun, J. Phys. Fluids **24**, 3650 (1983).
[22] R. W. Lee, B. L. Whitten, and R. E. Strout, J. Quant. Spectrosc. Radiat. Transfer **32**, 91 (1984).
[23] R. W. Lee, J. Quant. Spectrosc. Radiat. Transfer **40**, 561 (1988).
[24] Method described by B. L. Henke and M. A. Tester, in *Advances in X-Ray Analysis,* edited by W. L. Pickels (Plenum, New York, 1974), Vol. 18, p. 76; T. Kita, T. Harada, N. Nakano, and H. Kuroda, Appl. Opt. **22**, 512 (1983).
[25] B. L. Henke, L. L. Kwok, J. Y. Uejio, H. T. Yamada, and G. C. Young, J. Opt. Soc. Am. **1**, 817 (1984); B. L. Henke, J. Y. Uejio, G. F. Stone, C. H. Dittmore, and F. G. Fujiwara, *ibid.* **3**, 1540 (1986).

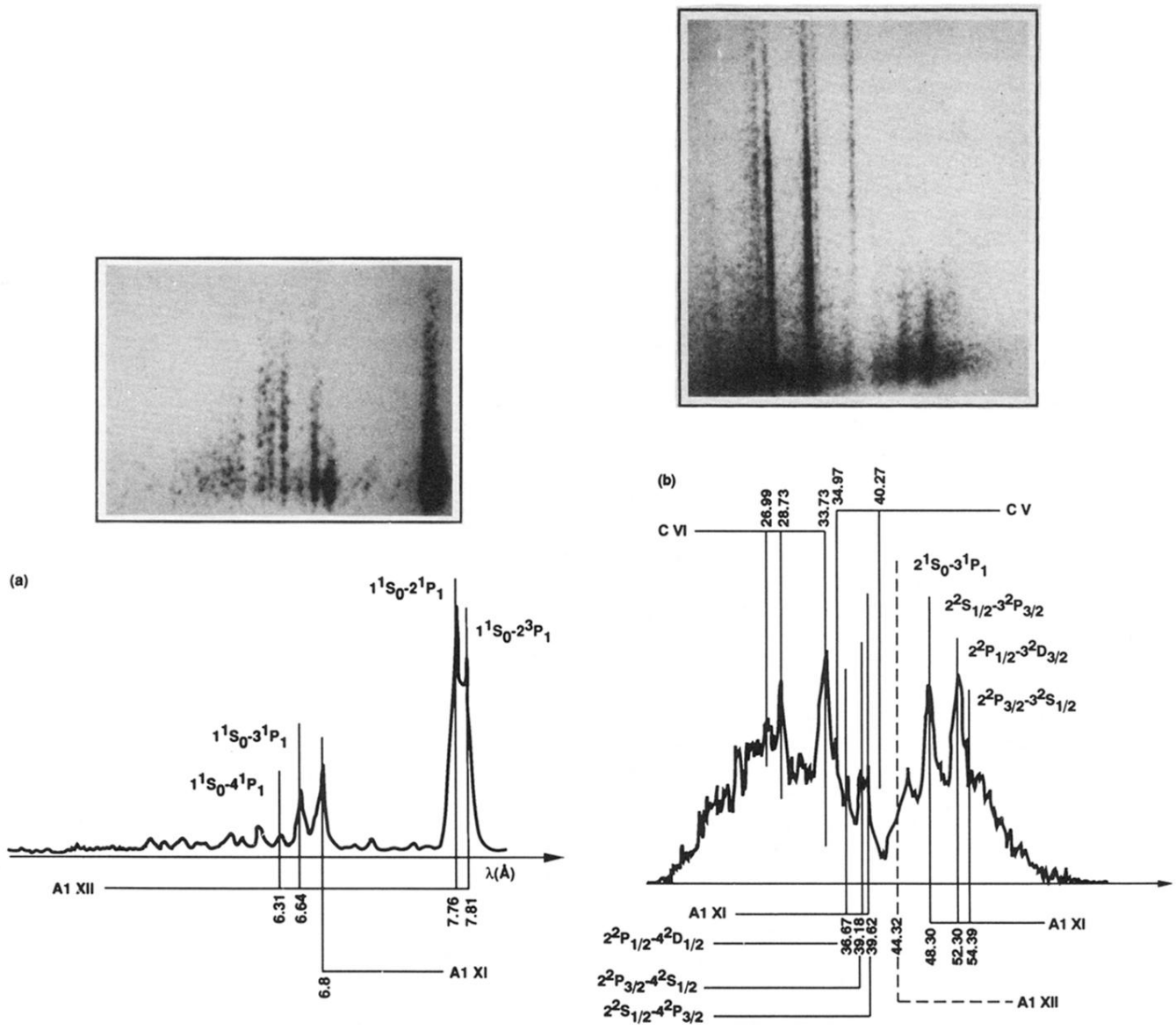

FIG. 4. Time-spectrally-resolved data recorded on x-ray streak cameras. (a) 4–8-Å wavelength region, (b) 20–60-Å wavelength region. The minimized emission of the He-like ions coupled with the strong emission of the Li-like ions indicates that the population of He-like ground-state ions is dominant.

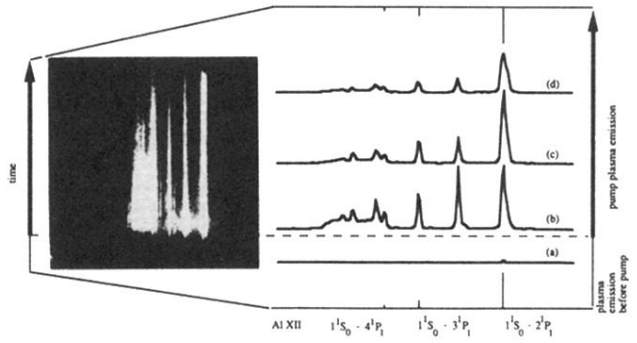

FIG. 5. Reference spectrum on the crystal streak camera in which the front and the pump plasma emission are both visible. The time axis is in bold after the creation of the pump. The front plasma is created by a 1.9-J, 1-ns pulse, focused into 600 μm, the pump is created by a 3.2-J, 100-ps pulse focused into 270 μm. (a) Self-emission of the plasma before the pump; (b) self-emission and pump emission at the peak of the pump; (c) 0.27 ns after the peak; (d) 0.53 ns after the peak.

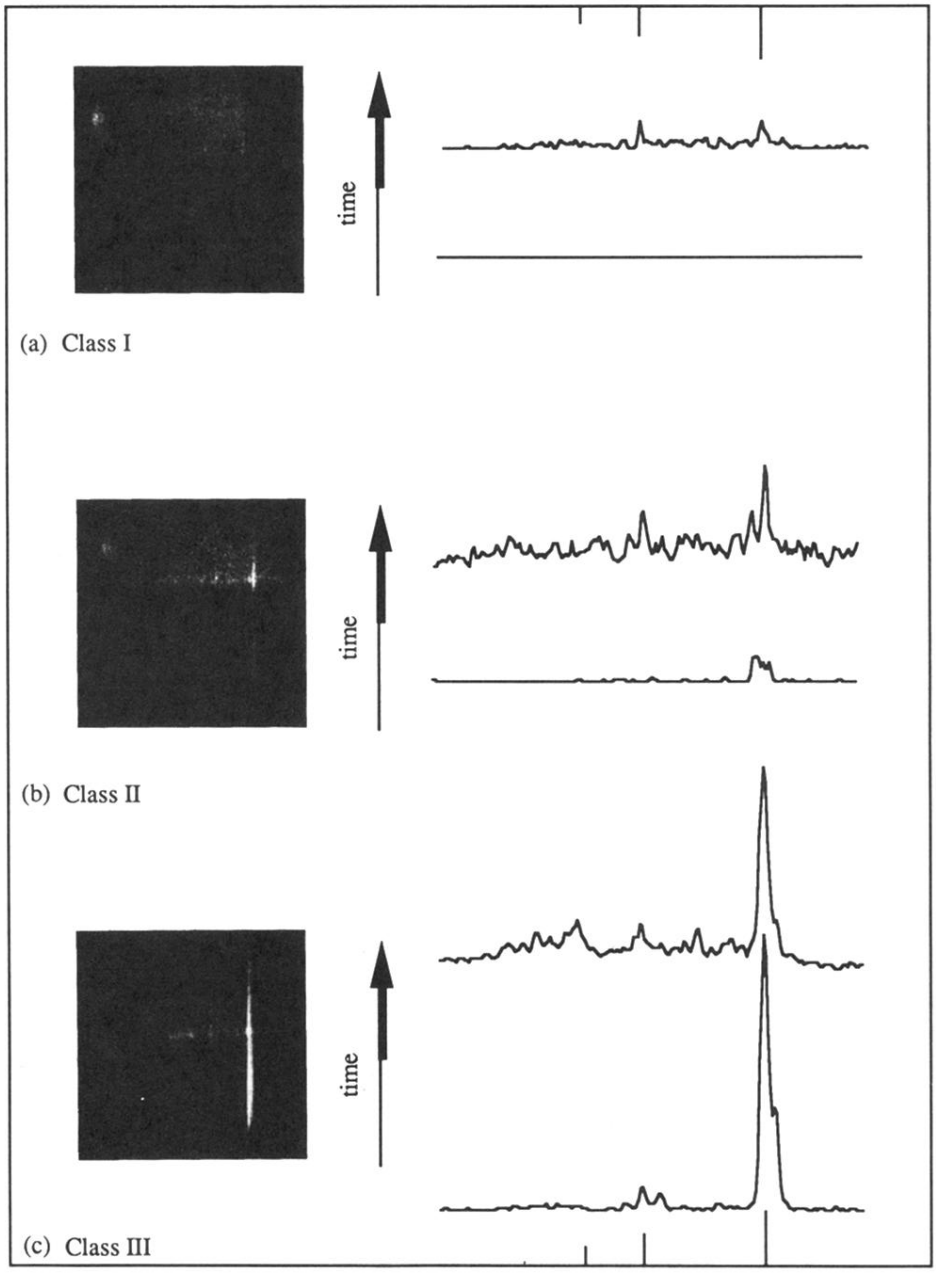

FIG. 6. Photographs of the raw data and the corresponding spectra showing the sensitivity of the fluorescence signal to the front plasma conditions. The time axis is shown in bold when the pump turns on. (a) Class I: little or no self-emission, the fluorescence is weak; (b) class II: self-emission that dies out before pump, the fluorescence signal is well separated in time; (c) class III: strong self-emission, the fluorescence appears on the tail.